Temperature-activated transition of positronium from self-trapped to delocalized state in CaF_2

K. Inoue,[1,*] N. Suzuki,[2,†] I. V. Bondarev,[3] and T. Hyodo[1]
[1]*Institute of Physics, Graduate School of Arts and Sciences, University of Tokyo, 3-8-1 Komaba, Meguro-ku, Tokyo 153-8902, Japan*
[2]*The Institute of Physical and Chemical Research (RIKEN), Hirosawa, Wako-shi, Saitama 351-0198, Japan*
[3]*Physics Department, North Carolina Central University, 1801 Fayetteville Street, Durham, North Carolina 27707, USA*
(Received 15 March 2007; published 10 July 2007)

Temperature dependence of the momentum distribution of positronium (Ps) in CaF_2 single crystal has been investigated in a temperature range from 10 to 297 K. Temperature activated transition of Ps from the stable self-trapped state to the metastable delocalized state has been observed. The self-trapping barrier height and the under-barrier tunnel self-trapping rate have been determined to be 0.17 eV and 2.9×10^{10} s^{-1}, respectively, and an important role of the under-barrier tunneling has been demonstrated. The bottom of the delocalized Ps band is 6.6 meV higher in energy than the ground self-trapped state. The observed effective mass of the delocalized Ps is considerably larger than the free Ps mass in vacuum.

DOI: 10.1103/PhysRevB.76.024304 PACS number(s): 78.70.Bj, 71.35.−y, 36.10.Dr

I. INTRODUCTION

Positronium (Ps), the bound state of a positron and an electron, forms in various dielectric crystals.[1] The Ps atom is sometimes regarded as an "isotope" of the exciton. Ps in solids couples to the phonon field, just as excitons do, resulting in a lattice distortion around itself.[2] Because it is neutral, Ps only interacts intensively with short-range acoustic and optic deformation potentials, not responding to long-range phonon-induced electric fields.[3,4]

Depending on the coupling strength to the short-range acoustic lattice vibrations and temperature, Ps has been observed to occupy two types of intrinsic states in dielectric crystals with low defect concentration. They are the Bloch-like ("free," delocalized) states and the self-trapped (localized on interstitial sites) states. For example, Ps in crystalline quartz (α-SiO_2),[5,6] ice,[7] and MgF_2 (Ref. 8) was observed to be delocalized in the broad temperature range from a few tens K up to a few hundreds K, whereas in typical alkali halide crystals, such as NaF, NaCl, NaI, KCl, KBr, and KI, the Ps was delocalized at temperatures below a few tens K, tending to be self-trapped with increasing temperature.[1] Quite an opposite tendency was observed for Ps in SrF_2 (Refs. 9 and 10), where the Ps was in the self-trapped states below 100 K, tending to be delocalized with increasing temperature.

The situation can be qualitatively understood in terms of the simplified configuration coordinate model for the self-trapping[11,12] shown in Fig. 1.[10–12] The short-range interaction between the Ps and the lattice distortion causes the adiabatic potential energy $U(Q)$ (Q being the continuous configuration coordinate representing the local lattice distortion around Ps) of the coupled Ps-lattice system to split off the continuum of the delocalized Ps states (thin lines in Fig. 1). When the Ps-phonon interaction is weak enough, the stable state of the Ps is the delocalized state with little lattice distortion. When the interaction is strong enough, the lowest Ps state can form a local minimum at $Q=Q_{st}$. This minimum represents the self-trapped state. The delocalized state and the self-trapped state are separated by the potential barrier of height U_b. The level of the self-trapped state $\varepsilon=B-E_{LR}$ is determined by the competition between the energy gained by the delocalization (given by the half-bandwidth B) and that gained by the lattice relaxation E_{LR} and can be higher or lower than the lowest delocalized state in the undeformed ($Q=0$) lattice, depending on whether the coupling constant

$$g=\frac{E_{LR}}{B} \tag{1}$$

is larger or smaller than unit. For example, the ground states of the excitons in alkali halides are known to be self-trapped with negative ε.[12] This is expected from the large excitonic band masses ($\sim10m$, m is the free electron mass) because a large band mass is associated with a small half-bandwidth B. For Ps, on the contrary, the sign of ε should depend on the type of the material because the Ps band mass [$\sim2.5m$ (Refs. 13 and 14)] is significantly smaller than that of the exciton in the same material.

The Ps in some alkali halides is one of the typical cases where the delocalized state is stable and the self-trapped state is metastable.[1] This has been revealed by the angular correlation of the annihilation radiation (ACAR). The ACAR measures the translational momentum distribution of the para-Ps (p-Ps) through the self-annihilation of the p-Ps. The ortho-Ps (o-Ps) does not give rise to the Ps peaks in the ACAR spectrum because it does not self-annihilate into two γ rays but dominately pick-off annihilates with an electron of the host material. Otherwise it behaves in a similar manner as the p-Ps does. At low temperatures (typically less than a few tens K), Ps populates mainly the delocalized states. In this case, very sharp peaks appear in the ACAR spectrum at zero momentum (main peak) and at the momenta corresponding to the reciprocal lattice vectors of the specimen crystal (satellite peaks), which reflect the Bloch nature of the translational wave function of Ps. As the temperature rises, Ps tends to be self-trapped. This results in a remarkable broadening of the main peak and diminishing satellite peaks in the ACAR spectrum, indicating the temperature activated transition of the delocalized Ps to the self-trapped states.

Recently, Inoue, Suzuki, and Hyodo[9] have revealed the temperature activated transition from the self-trapped to the

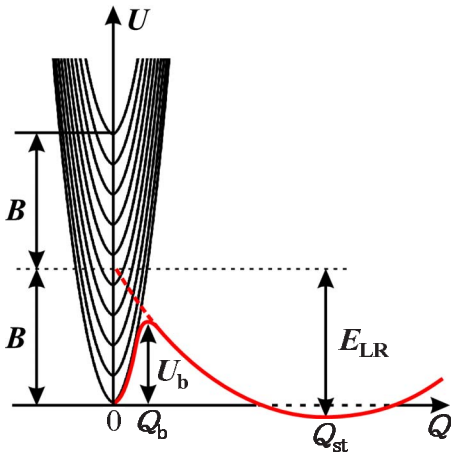

FIG. 1. (Color online) Schematic of the adiabatic potential energy U of the coupled Ps-lattice system as a function of the configurational coordinate Q representing the local lattice distortion around the Ps (Ref. 10).

delocalized state in the SrF_2 single crystal. This is the case illustrated in Fig. 1 where the self-trapped state of Ps is stable and the delocalized state is metastable. Later on, Bondarev *et al.*[10] have demonstrated an important role of the temperature activated tunnel (underbarrier) detrapping mechanism for the self-trapped Ps in SrF_2. The bottom of the delocalized Ps band (the metastable lowest delocalized state) in SrF_2 was shown to be just a hundredth fraction of meV higher in energy than the stable self-trapped state. Therefore, the self-trapped Ps tends to occupy the continuum of the delocalized states with increasing temperature by tunneling through and hopping over the self-trapping barrier at low and high temperatures, respectively.

CaF_2, which is an alkaline earth fluoride like SrF_2, is commonly used as a window material for both infrared and ultraviolet wavelengths, since it is transparent in these regions and exhibits extremely weak birefringence. It is particularly important as an ultraviolet optical material for integrated circuit lithography. Coussot[15] measured the ACAR spectrum for CaF_2 single crystal at room temperature and found the satellite peaks appearing at the momenta corresponding to the reciprocal lattice vectors. Kasai[16] measured the ACAR spectrum for CaF_2 at 10 K; no sharp delocalized Ps peak was observed. Temperature dependence of the momentum distribution of Ps in CaF_2, however, has not been investigated yet. In the present work we apply the ACAR technique to investigate the momentum distribution of Ps in CaF_2 in the temperature range from 10 K up to 297 K. Our measurements show that the ground state of the Ps in CaF_2 is the self-trapped state whereas the (barrier-separated) delocalized states form the continuum of the delocalized states. We observe the transition of the self-trapped Ps to the delocalized states with increasing temperature.

II. EXPERIMENTAL PROCEDURE

High resolution one-dimensional (1D) ACAR measurements have been performed on CaF_2. The sample CaF_2 single crystal used was supplied by OKEN Co. Ltd.

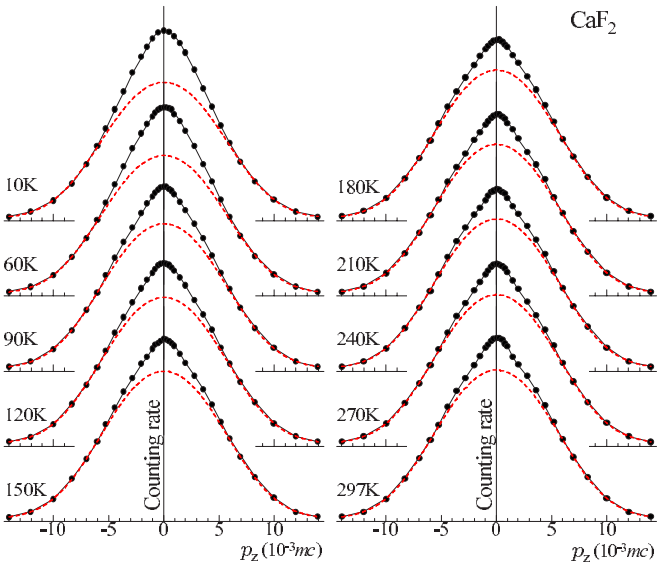

FIG. 2. (Color online) Momentum distributions of the annihilation photons along the ⟨100⟩ axis of CaF_2 in the temperature range 10–297 K. The broken lines indicate the common broad component representing the monomentum distribution of the electrons in CaF_2.

The 1D projection of the electron-positron momentum distribution onto the ⟨100⟩ direction of the crystal was measured in the temperature range from 10 K to room temperature under a magnetic field of +1.1 T. The positive (negative) sign indicates the direction of the field parallel (antiparallel) to the positron incident direction. The momentum resolution was $0.45\times10^{-3}mc$ (c is the speed of light, $mc=137$ atomic unit of momentum) full-width at half-maximum (FWHM). The specimen temperature was controlled to within ±0.5 K at values below room temperature. Measurements were also performed at room temperature, 297±1 K. In order to confirm that Ps is definitely formed, momentum distribution was also measured in a magnetic field of −1.1 T at several temperatures.[17] Confirmation of the Ps formation by this method is based on the fact that the positrons emitted from a β^+ decay source are spin-polarized along their momenta. The 2γ self-annihilation of the Ps is more enhanced when the magnetic field is parallel to the positron spin than antiparallel.[17]

III. EXPERIMENTAL RESULTS

The momentum distributions obtained at various temperatures by the 1D-ACAR measurements are shown in Fig. 2, where the 2γ coincidence counting rate is plotted against momentum p_z. The data is found to be temperature dependent; a cusplike structure, which is not observed at 10 K, is seen at the center of the momentum distributions at temperatures above 90 K.

Figure 3 shows the result of the subtraction of the momentum distributions in the magnetic field −1.1 T from those taken in +1.1 T. The detailed method of the subtraction is described elsewhere.[17] The remaining component gives the momentum distribution of Ps, clearly evidencing the exis-

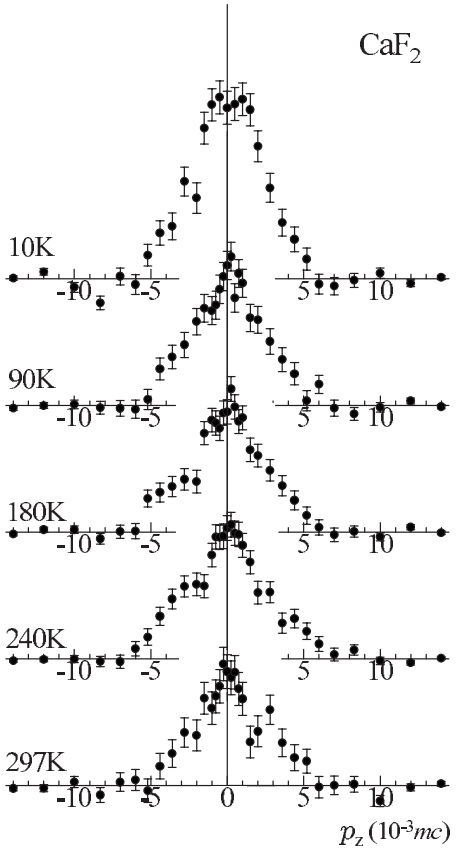

FIG. 3. Positronium momentum distribution in CaF_2 obtained using the effect of the positron spin-polarization on Ps formation.

tence of Ps in CaF_2. The Ps momentum distributions above 90 K shown in Fig. 3 appears to be composed of two components, a very narrow component at around zero momentum and a wider component, while the Ps momentum distribution at 10 K seems to be composed of only one component. The narrow component above 90 K gives rise to the cusp noticeable in the raw 1D-ACAR data shown in Fig. 2. The Ps momentum distribution at 10 K is approximated by a single Gaussian function of FWHM $5.9\times10^{-3}mc$.

In order to investigate the temperature dependence of the Ps components more precisely, we subtracted from every curve a common broad component which resulted from the annihilation of the positrons with electrons of the CaF_2 without forming Ps and the pick-off annihilation of Ps. The shape of the momentum distribution, $F(p_z)$, was reproduced by

$$F(p_z) = F_1(p_z) + F_2(p_z) + F_3(p_z), \tag{2}$$

where

$$F_1(p_z) = a\exp(-\alpha p_z^2),$$

$$F_2(p_z) = b\exp(-\beta p_z^2),$$

$$F_3(p_z) = d\{\exp[-\xi(p_z-h)^2] + \exp[-\xi(p_z+h)^2]\}.$$

The parameters a, b, d, h, α, and ξ are determined by fitting the function (2) simultaneously to the three 1D-ACAR data results at 120, 210, and 297 K. The function $F_1(p_z)$ represents the narrower Ps component, $F_2(p_z)$ represents the broader Ps component, and $F_3(p_z)$ represents the shape of the common broad component. A rather unusual function $F_3(p_z)$ with temperature independent parameters ξ and h was introduced after we have found that a sum of two Gaussians commonly centered at zero momentum did not give a good fit. The parameters ξ and h have no physical meaning, but are introduced just to reproduce the broad component. A constraint of the fitting was that the parameter β was fixed to give a width of $5.9\times10^{-3}mc$, as determined in the magnetic quenching experiments. This component is due to the self-annihilation of the Ps in a localized state. The fitted values for $\xi(=4\ln 2/W^2, W=9.5\times10^{-3}mc)$ and $h(=2.8\times10^{-3}mc)$ give reasonable shape for the broad component as shown by the broken lines in Fig. 2, i.e., the shape is not bimodal as would be if the values for h were not small. The parameter α was dependent on the temperature. The Ps component $F_1(p_z)+F_2(p_z)$, which was isolated by subtracting the obtained common broad component $F_3(p_z)$ from each of the momentum distributions is shown in Fig. 4 together with the fitted $F_2(p_z)$.

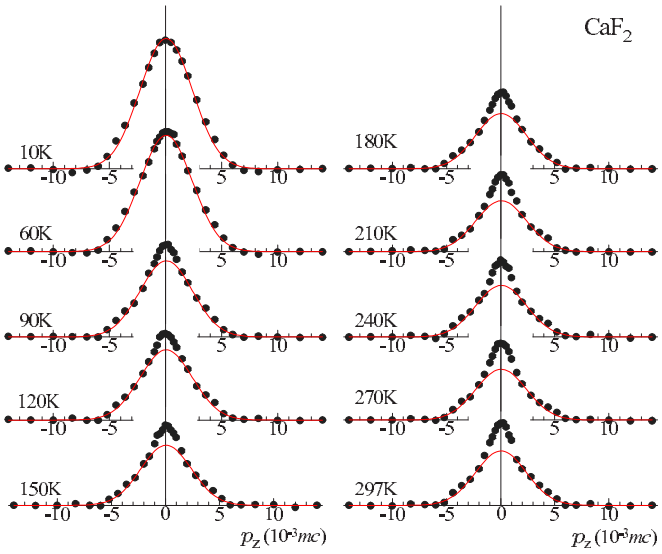

FIG. 4. (Color online) Temperature dependence of the Ps momentum distribution in CaF_2 obtained by subtracting the common broad component from the momentum distribution in Fig. 2. The solid lines indicate the component of Ps in the localized state.

IV. DISCUSSION

Figure 5 shows the component $F_1(p_z)$ obtained by subtracting the fitted function, $F_2(p_z)+F_3(p_z)$, from the ACAR spectrum at 297 K. The main peak at the zero momentum and the satellite peaks at around $\pm4.5\times10^{-3}mc$ and around $\pm8.5\times10^{-3}mc$ are seen. The positions of the satellite peaks correspond to the projections of the reciprocal lattice vectors $\mathbf{G}_{1kl}$ and $\mathbf{G}_{2kl}$ (k,l are indices in the reciprocal lattice vector) onto the $\langle100\rangle$ direction of the CaF_2 single crystal; G in the figure indicates the momentum corresponding to the nearest reciprocal lattice vector $\hbar G_{100}(=4.44\times10^{-3}mc)$. These Ps peaks are due to the self-annihilation of the delocalized Ps.

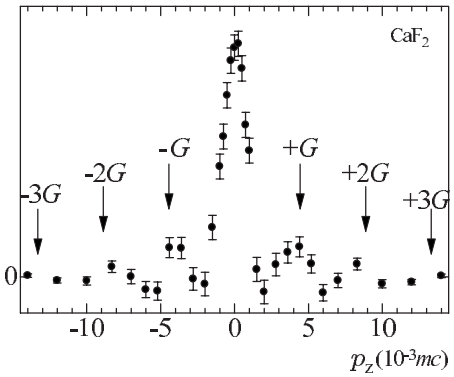

FIG. 5. Momentum distribution of delocalized Ps at 297 K in CaF_2. The G represents the momentum corresponding to the projection of the nearest reciprocal lattice vector of CaF_2 crystal.

The relative intensities of the satellite peaks to the main peak are 0.13 ± 0.02 for $\pm G$ and 0.06 ± 0.02 for $\pm 2G$.

Figure 6 shows the temperature dependence of W_1^2, the square of the FWHM of the central narrow Ps component $F_1(p_z)$. The function $W_1^2(T)$ increases with temperature and becomes flat at around 200 K.

The temperature dependence of the Ps components shown in Fig. 4 indicates that the temperature activated transition of the Ps from the localized to the delocalized states takes place in CaF_2 in a similar manner as it does in SrF_2.[9,10] The fractional intensity of the delocalized Ps component $S_1/(S_1+S_2)$ is plotted against temperature in Fig. 7, where S_1 and S_2 are the intensities of the delocalized and the localized Ps components, respectively. The fractional intensity of the delocalized Ps component increases with temperature and becomes flat at around 200 K.

Both the FWHM and the fractional intensity of the delocalized Ps component become flat at temperatures above ~200 K. To understand these behaviors, we use the theoretical momentum distribution in terms of the many-particle Green's function formalism[18]

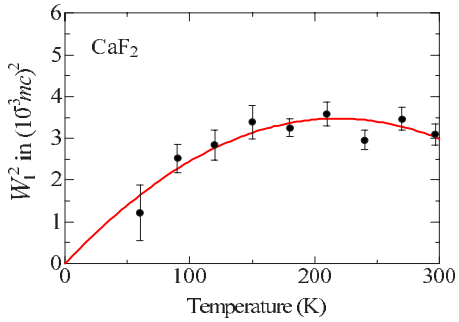

FIG. 6. (Color online) Temperature dependence of the square of the width (FWHM) of the delocalized Ps component in CaF_2. The width has been corrected for the broadening due to the optical resolution of the apparatus. The solid line represents the least-squares fitted curve assuming that the effective mass depends linearly on temperature.

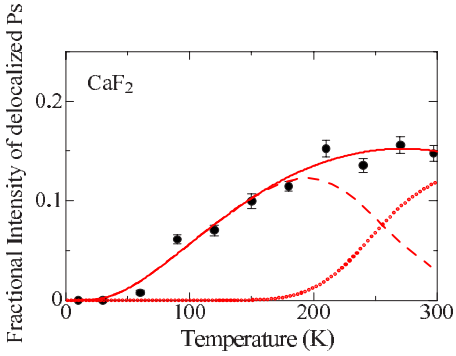

FIG. 7. (Color online) Temperature dependence of the delocalized Ps fraction in CaF_2: full circles show the experimental data; solid line is the list-squares fitted theoretical curve given by Eqs. (7)–(10) with $\varepsilon=6.6$ meV, $U_b=0.17$ eV, $\Gamma=2.9\times10^{10}$ s^{-1}, and $x=0.3$; the dashed line and the dotted line show the contributions from the tunnel detrapping and classical activation detrapping, respectively.

$$N(p) \sim \int_0^\infty d\omega e^{-\omega/k_BT} \frac{\Gamma(\mathbf{p},\omega)}{[\omega - \mathbf{p}^2/2M^* - \Delta(\mathbf{p},\omega)]^2 + \Gamma^2(\mathbf{p},\omega)}, \tag{3}$$

where the exponential factor stands for the Boltzmann statistics, and the Ps chemical potential is taken to be zero because there is at most only one Ps at a time under usual experimental conditions. The nonexponential factor stands for the so-called spectral density function of the thermalized Ps interacting with the field of longitudinal acoustic phonons at finite temperatures; $\Gamma(\mathbf{p},\omega)$ and $\Delta(\mathbf{p},\omega)$ are the imaginary and real self-energies of Ps with the quasimomentum $\mathbf{p}$ and the band mass M^*. In the weak Ps-phonon coupling regime (delocalized Ps—see Ref. 13), one can utilize the second-order-interaction finite temperature renormalization technique and, following Ref. 19, approximate the momentum distribution in Eq. (3) by the Gaussian function of the form

$$N(p) \approx \exp\left[-\frac{\mathbf{p}^2}{2M^{**}(T)k_BT}\right], \tag{4}$$

with the effective mass M^{**} given by

$$M^{**}(T) = M^* \frac{1 - a_1 T}{(1 + a_2 T)(1 - bT)}, \tag{5}$$

where a_1 and a_2 are the (temperature independent) mass renormalization constants originating from the real Ps self-energy $\Delta(\mathbf{p},\omega)$, and b is the temperature independent parameter coming from the imaginary Ps self-energy $\Gamma(\mathbf{p},\omega)$. The constants $a_{1,2}$ and b are all positive, small in their values, and determined by the matrix element of the Ps interaction with the longitudinal acoustic vibrations along with the lattice parameters such as the Debye temperature, the lattice constant, the elementary cell mass, the sound velocity, etc.[13,19] The effective mass in Eq. (5) is the so-called "visible" Ps mass.[19] This mass is different from that in the commonly used quasiparticle polaron model where the polaron mass and the damping of the quasiparticle polaron state are contributed

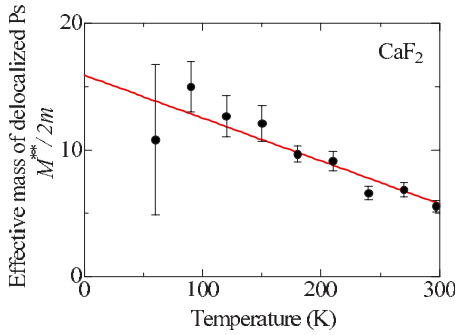

FIG. 8. (Color online) Temperature dependence of the effective mass of the delocalized Ps in CaF_2. The solid line represents the least-squares fitted line assuming that the effective mass depends linearly on temperature.

independently by $\Delta(\mathbf{p},\omega)$ and $\Gamma(\mathbf{p},\omega)$, respectively.[18]

The FWHM of the delocalized Ps momentum distribution is estimated from Eq. (4) to be

$$W_1 = [8(\ln 2)M^{**}(T)k_BT]^{1/2}. \tag{6}$$

The function W_1^2/k_BT may be temperature independent, so that W_1^2 increases linearly with temperature, when the contributions of the real and imaginary self-energies in Eq. (5) approximately compensate each other. Such a situation was observed in many alkali halide crystals.[1] On the other hand, when either the imaginary self-energy or the real self-energy contribution dominates Eq. (5) over a specific temperature range, the function W_1^2/k_BT may, respectively, be increasing or decreasing with temperature in this temperature range, yielding a nonlinear temperature dependence of W_1^2. The former situation is very well known for the delocalized Ps in crystalline SiO_2 (Ref. 19) and in MgF_2,[3] whereas the latter one seems to be the case for Ps in CaF_2 as one can see in Fig. 6 above ~150 K.

We have estimated the temperature dependence of the delocalized Ps effective mass from Eq. (6) using the experimental values of $W_1(T)$ (shown in Fig. 6) and $M^{**}(T)$ given by Eq. (5) under the assumption that $b \ll a_{1,2} \ll 1$. The result is shown in Fig. 8 with the solid straight line representing the linear dependence $M^{**}(T)=15.9(1-2.12\times10^{-3}T)\times 2m$. We further used this $M^{**}(T)$ to fit the data for the fractional intensity of the delocalized Ps component shown in Fig. 7 in terms of the model that takes into account the self-trapping potential barrier and the under-barrier tunneling effect between the delocalized and the self-trapped Ps states (see Fig. 1). The model was proposed by Bondarev and Hyodo[20] to explain the low-temperature behavior of the self-trapped Ps fraction of the delocalized Ps atoms in alkali halides, and was recently adapted to explain the temperature dependence of the delocalized Ps fraction of the self-trapped Ps in SrF_2.[10] The delocalized Ps fraction is given within this model by

$$f_F = \frac{\lambda_f^{SA}\gamma_f}{\lambda_t^{SA}(\lambda_f+\gamma_t)+\lambda_f^{SA}\gamma_f}, \tag{7}$$

where λ_f^{SA}, λ_t^{SA}, γ_t, and γ_f are the self-annihilation rate of Ps in the free delocalized state, that in the self-trapped state, the trapping rate from the delocalized state to the self-trapped state, and the detrapping rate from the self-trapped state to the delocalized state, respectively. $\lambda_f(=\lambda_f^{SA}+\lambda_f^{PO})$ is the annihilation rate of Ps in the delocalized state with the pick-off annihilation process (λ_f^{PO}) taken into account. The self-trapping rate is contributed by the (classical) activation type over-barrier self-trapping mechanism and by the tunnel under-barrier self-trapping mechanism, yielding γ_t in the form

$$\gamma_t = \nu \exp\left(-\frac{U_b}{k_BT}\right) + \Gamma, \tag{8}$$

where $\nu=\omega/2\pi$ is the typical phonon frequency associated with the local lattice deformation, U_b is the height of the self-trapping barrier seen by the delocalized Ps (see Fig. 1) and Γ is the rate of the under-barrier tunnel escape (tunnel self-trapping rate) of the delocalized Ps into the ground self-trapped state. The detrapping rate γ_f can then be estimated from the statistical detailed balance equation

$$\gamma_f g_t = \gamma_t g_f(T)\exp\left(-\frac{\varepsilon}{k_BT}\right), \tag{9}$$

yielding

$$\gamma_f = \frac{g_f(T)}{g_t}\left[\nu \exp\left(-\frac{U_b+\varepsilon}{k_BT}\right) + \Gamma \exp\left(-\frac{\varepsilon}{k_BT}\right)\right], \tag{10}$$

with $\varepsilon=E_{LR}-B>0$ being the energy difference between the delocalized and the self-trapped Ps states (see Fig. 1), $g_f(T)=\Sigma_{\mathbf{p}}\exp[-\mathbf{p}^2/2M^{**}(T)k_BT]=V[M^{**}(T)k_BT/2\pi\hbar^2]^{3/2}$ representing the effective number (the statistical weight) of the delocalized Ps states occupied at temperature T, and $g_t=x(V/v_0)$ standing for the number of possible localization sites for the Ps in the crystal of volume V, where $v_0=a^3$ is the elementary cell volume with $a=5.46$ Å (Ref. 21) and x is the number of possible trapping sites in an elementary cell. The two items in the brackets represent the contributions of the classical activation type detrapping mechanism and that of the tunnel detrapping mechanism, respectively.

We simplified Eq. (7) by assuming that $\lambda_f=8\times10^9$ s^{-1} (same as the free para-Ps annihilation rate in vacuum), $\lambda_f^{SA}=\lambda_t^{SA}$, and $\nu=\omega_D/2\pi$ where the Debye frequency $\omega_D=k_BT_D/\hbar$ with $T_D=508$ K.[22] The delocalized Ps fraction f_F was then fitted to the data with ε, U_b, Γ, and x being adjustable parameters. The least-squares-fitting gives

$$\varepsilon = 6.6 \pm 0.5 \text{ meV},$$

$$U_b = 0.17 \pm 0.01 \text{ eV},$$

$$\Gamma = (2.9 \pm 0.1)\times 10^{10} \text{ s}^{-1},$$

and $x=0.30\pm0.01$. The corresponding fitting curve is shown by the solid line in Fig. 7. The dashed curve and the dotted curve show the contribution of the under-barrier tunnel detrapping and that of the over-barrier classical detrapping, respectively. The tunnel detrapping mechanism is seen to be very important in the temperature range from several tens K up to 250 K, whereas the classical detrapping mechanism

dominates at higher temperatures above 250 K. The tunnel detrapping parameters obtained, U_b and Γ, are very close to those in SrF_2.[10]

The energy difference, ε, between the lowest delocalized state and the self-trapped state of Ps in CaF_2 is more than two orders of magnitude larger than that for Ps in SrF_2,[10] indicating, according to Fig. 1, that E_{LR} is larger and B is smaller in CaF_2 than those in SrF_2, thereby yielding the stronger Ps-phonon coupling in CaF_2 compared to that in SrF_2, according to Eq. (1). The fact that the delocalized Ps half-bandwidth B in CaF_2 is smaller than that in SrF_2 is consistent with the experimental observations of the larger "visible" effective mass of the delocalized Ps in CaF_2 than that in SrF_2 [$\sim 20m$ in CaF_2, see Fig. 8, against $\sim 12m$ in SrF_2 (Ref. 9)]. The fact that the lattice relaxation energy E_{LR} is larger in CaF_2 than that in SrF_2 is supported by the obvious argument that E_{LR} is inversely proportional to the elementary cell mass of the crystal lattice[11] which is smaller in CaF_2 than in SrF_2.

The localized Ps state in CaF_2 is the intrinsic self-trapped state, judging from the fitted number of the self-trapped states $g_t = x(V/v_0) \approx 0.3(V/v_0)$ which is of the order of the lattice cells in the crystal. Extrinsic self-trapping is associated with defects;[12] it would yield much smaller number of self-trapping sites than that we obtained.

We neglected the temperature dependence of the tunnel self-trapping rate Γ in the considerations above. This is partly justified by the large Debye temperature of 508 K of crystalline CaF_2. According to the instanton approach to the theory of nonradiative transitions (see Ref. 23), the tunnel self-trapping rate by the acoustic mode of lattice vibrations at $T < T_D$ is of the form $\Gamma(T) \sim \Gamma_0(1 - T/T_D)^{-3/2} \exp[C(T/T_D)^4]$ with C being a constant depending on elastic properties of the crystal. Thus, for $T \sim 100$ K the tunnel self-trapping rate in CaF_2 can be roughly regarded to be temperature-independent to simplify the analysis of experimental data.

V. SUMMARY

We have investigated the temperature dependence of the momentum distribution of the positronium in CaF_2 single crystal in the temperature range from 10 to 297 K. The temperature activated transition of Ps from the stable self-trapped state to the metastable delocalized state, which was earlier observed in SrF_2,[9,10] has been now observed in CaF_2. The parameters of the Ps self-trapping process, such as the self-trapping barrier height and the under-barrier tunnel self-trapping rate, have been determined to be 0.17 eV and 2.9×10^{10} s^{-1}, respectively, and an important role of the under-barrier tunneling has been demonstrated. The bottom of the delocalized Ps band is about seven meV higher in energy than the ground state of the self-trapped Ps. The observed effective mass of delocalized Ps is considerably larger than the free Ps mass in vacuum and linearly decreases with temperature. We interpret this effect in terms of the Ps interaction with long wavelength longitudinal acoustic lattice vibrations.

ACKNOWLEDGMENTS

We thank H. Saito for his support during the experiments.

*Present address: The Oarai Center, Institute for Materials Research, Tohoku University, Oarai, Ibaraki 311-1313, Japan. kinoue@imr.tohoku.ac.jp

†Present address: ISIR-SANKEN, Osaka University, Mihogaoka 8-1, Ibaraki, Osaka 567-0047, Japan.

[1] J. Kasai, T. Hyodo, and K. Fujiwara, J. Phys. Soc. Jpn. **57**, 329 (1988).

[2] I. V. Bondarev and T. Hyodo, Acta Phys. Pol. A **107**, 673 (2005).

[3] I. V. Bondarev, Y. Nagai, M. Kakimoto, and T. Hyodo, Phys. Rev. B **72**, 012303 (2005).

[4] I. V. Bondarev, Nucl. Instrum. Methods Phys. Res. B **221**, 230 (2004).

[5] H. Ikari and K Fujiwara, J. Phys. Soc. Jpn. **46**, 92 (1979).

[6] H. Saito and T. Hyodo, Phys. Rev. Lett. **90**, 193401 (2003).

[7] O. E. Mogensen, G. Kvajic, M. Eldrup, and M. M. Kvajic, Phys. Rev. B **4**, 71 (1971).

[8] Y. Nagai, M. Kakimoto, T. Hyodo, K. Fujiwara, H. Ikari, M. Eldrup, and A. T. Stewart, Phys. Rev. B **62**, 5531 (2000).

[9] K. Inoue, N. Suzuki, and T. Hyodo, Phys. Rev. B **71**, 134305 (2005).

[10] I. V. Bondarev, K. Inoue, N. Suzuki, and T. Hyodo, Phys. Status Solidi B (to be published).

[11] Y. Toyozawa, *Optical Processes in Solids* (Cambridge University Press, Cambridge, 2003).

[12] M. Ueta, H. Kanzaki, K. Kobayashi, Y. Toyozawa, and E. Hanamura, *Excitonic Processes in Solids* (Springer, New York, 1986).

[13] I. V. Bondarev, Phys. Rev. B **58**, 12011 (1998).

[14] A. B. Kunz and J. T. Waber, Solid State Commun. **39**, 831 (1981).

[15] G. Coussot, Ph.D. thesis, University of Paris, Paris, 1970.

[16] J. Kasai, Ph.D. thesis, University of Tokyo, Tokyo, 1983.

[17] T. Hyodo, M. Kakimoto, Y. Nagashima, and K. Fujiwara, Phys. Rev. B **40**, 8037 (1989).

[18] G. Mahan, *Many-Particle Physics* (Plenum, New York, 1993).

[19] H. Ikari, J. Phys. Soc. Jpn. **46**, 97 (1979).

[20] I. V. Bondarev and T. Hyodo, Phys. Rev. B **57**, 11341 (1998).

[21] *Handbook of Chemistry and Physics*, edited by D. R. Lide (CRC Press, New York, 1999).

[22] D. R. Huffman and M. H. Norwood, Phys. Rev. **117**, 709 (1960).

[23] A. S. Ioselevich and E. I. Rashba, J. Lumin. **34**, 223 (1986).